Regolith Migration and Sorting on Asteroid Itokawa

Hideaki Miyamoto,[1,2,3,4]* Hajime Yano,[5] Daniel J. Scheeres,[6] Shinsuke Abe,[7] Olivier Barnouin-Jha,[8] Andrew F. Cheng,[8] Hirohide Demura,[9] Robert W. Gaskell,[10] Naru Hirata,[9] Masateru Ishiguro,[11] Tatsuhiro Michikami,[12] Akiko M. Nakamura,[7] Ryosuke Nakamura,[13] Jun Saito,[5,14] Sho Sasaki[15]

High-resolution images of the surface of asteroid Itokawa from the Hayabusa mission reveal it to be covered with unconsolidated millimeter-sized and larger gravels. Locations and morphologic characteristics of this gravel indicate that Itokawa has experienced considerable vibrations, which have triggered global-scale granular processes in its dry, vacuum, microgravity environment. These processes likely include granular convection, landslide-like granular migrations, and particle sorting, resulting in the segregation of the fine gravels into areas of potential lows. Granular processes become major resurfacing processes because of Itokawa's small size, implying that they can occur on other small asteroids should those have regolith.

The degree to which small asteroids are covered by regolith (*1*) is an important unanswered question with implications for the evolution of these bodies. Formation of regolith on asteroids is different from that on the Moon (*2*) because of substantial differences in surface accelerations. Whereas repetitious impacts on the Moon form locally concentrated, size-sorted regolith, impact ejecta on an asteroid are ballistically spread over the entire surface to form globally continuous, generally uniform, and poorly sorted regolith with large fractions of escaping ejecta (*2*). However, the small (~300-m diameter) near-Earth asteroid Itokawa (*3*) has a considerable amount of regolith distributed nonuniformly. This poses the fundamental question of how the regolith has been segregated. Because Itokawa is by far the smallest asteroid ever studied at high resolution, previously unrecognized processes of regolith evolution may be active.

In November 2005, the Hayabusa spacecraft performed touchdown rehearsals, imaging navigation tests, and two touchdowns on Itokawa (*4*). These provided close-up images of Itokawa, mostly on the east side (fig. S1) at ranges below 2 km and down to 63 m, where image resolution was 6 mm per pixel (Figs. 1 to 3). Close-up images reveal the surface to be covered with unconsolidated gravels (*5*), which are typically piled on each other without being buried by fines (Figs. 1 to 3). These unconsolidated gravels commonly have the following two characteristics regardless of location: None of the smaller gravels in close-up images are isolated on top of boulders without being supported by other gravels (Figs. 1C and 2), and the position and orientation of gravels are apparently stable against local gravity (Figs. 1C, 2, and 3B). These give a strong indication that gravels on the surface of Itokawa were reallocated after their accumulation/deposition, implying that the surface has been subject to global vibrations. Vibrations are also suggested by the shapes of craters that are generally obscured on Itokawa (*6*) and often associated with partially disrupted rims (Fig. 1, A and D). These vibrations may have been caused by impact-induced seismic shaking (*7*, *8*), because a centimeter-sized impactor can globally induce seismic acceleration on Itokawa as large as its surface gravity (Fig. 4A). Other possible reasons for vibrations include tidal effects, thermally induced mechanical fluctuations, or low-speed collisions between the head and the body (*3*) due to a high spin rate of the asteroid in the past (*9*).

Grain sizes observed in close-up images range from centimeters to several tens of meters. The finest particles are centimeter-sized pebbles, whose concentrations are found in the Muses-C smooth terrain (Fig. 3A and fig. S1). Although powdery materials are thought to be created through impact processes (*10*–*12*), they might have been electrostatically levitated and removed by solar radiation pressure (*13*, *14*), had much higher ejection velocity after impacts to restrict their reaccumulations (*10*), or been segregated into the interior.

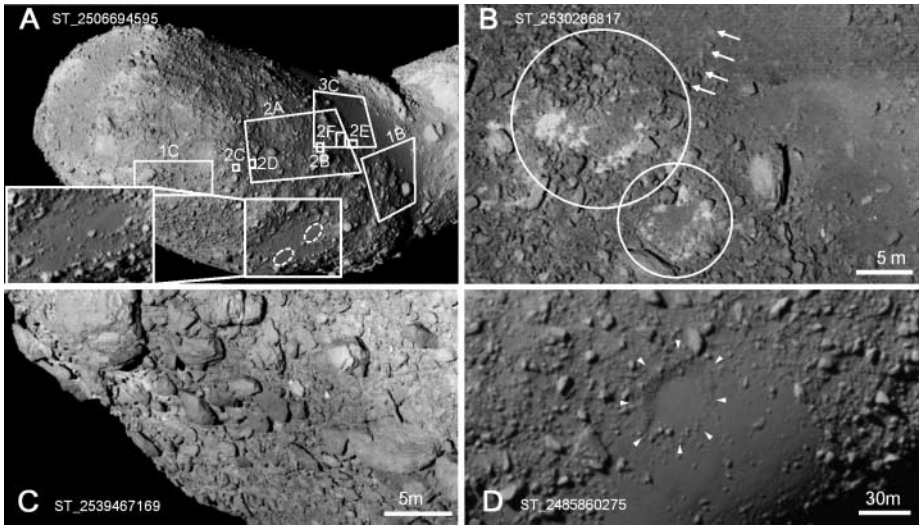

Fig. 1. (**A**) Locations of close-up images (number and letter of the figure where each image is shown). Inset shows the Uchinoura smooth terrain, which is likely formed by a single crater or a cluster of craters (dotted circles). Note the disrupted crater rims and flattened floors filled by fine gravels. (**B**) Piles of gravels with craterlike depressions (circles) (see fig. S2). Debris of a collapsed rim drained into the smooth terrain (arrows), which is a gravitational low. (**C**) Rounded boulders are sitting in stable orientations against local gravity. (**D**) A crater candidate in the Sagamihara smooth terrain with the disrupted rim (triangles) and the flat floor. In all images, numbers starting with "ST_" indicate their image frames. Upper portions of some images are obscured by the onboard polarizer (*6*).

[1]Department of Museum Collection Utilization Studies, The University Museum, University of Tokyo, Hongo 7-3-1, Bunkyo-ku, Tokyo 113-0033, Japan. [2]Department of Earth and Planetary Science, University of Tokyo, Hongo 7-3-1, Bunkyo-ku, Tokyo 113-0033, Japan. [3]Department of Geosystem Engineering, University of Tokyo, Hongo 7-3-1, Bunkyo-ku, Tokyo 113-8656, Japan. [4]Planetary Science Institute, 1700 East Fort Lowell Road, Suite 106, Tucson, AZ 85719, USA. [5]Institute of Space and Astronautical Science, Japan Aerospace Exploration Agency, 3-1-1 Yoshinodai, Sagamihara, Kanagawa 229-8510, Japan. [6]Department of Aerospace Engineering, University of Michigan, Ann Arbor, MI 48109, USA. [7]Graduate School of Science and Technology, Kobe University, 1-1 Rokkodai-cho, Nada-ku, Kobe 657-8501, Japan. [8]Johns Hopkins University Applied Physics Laboratory, Laurel, MD 20723, USA. [9]Department of Computer Software, University of Aizu, Ikki-machi, Aizu-Wakamatsu City, Fukushima 965-8580, Japan. [10]Jet Propulsion Laboratory, California Institute of Technology, Pasadena, CA 91109, USA. [11]Astronomy Department, Seoul National University, Seoul 151-747, Korea. [12]Fukushima National College of Technology, Iwaki 970-8034, Japan. [13]National Institute of Advanced Industrial Science and Technology, Tsukuba 306-8568, Japan. [14]School of Engineering, Tokai University, Hiratsuka, Kanagawa 259-1292, Japan. [15]Research in Selenodesy Project Office, National Astronomical Observatory of Japan, 2-12 Hoshigaoka, Mizusawa, Oshu 023-0861, Japan.

*To whom correspondence should be addressed. E-mail: hm@um.u-tokyo.ac.jp

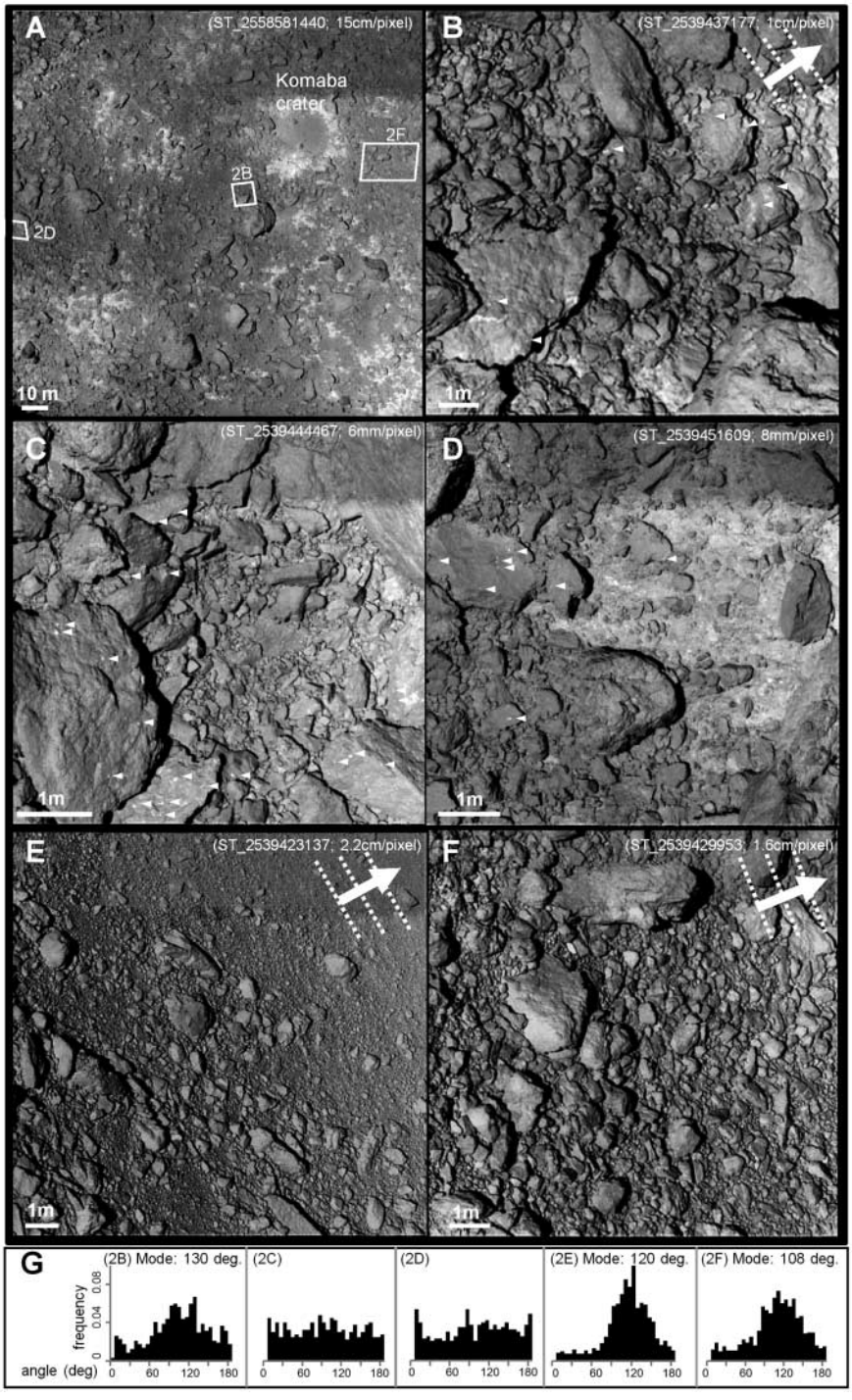

Fig. 2. (**A**) The rough terrain around the Komaba crater (Fig. 1A), showing locations of individual close-up images. (**B**) Gravels are weakly organized in the direction of the dotted lines. Bright dots (triangles) are observed on gravels of various sizes. (**C**) Larger gravels generally overlie smaller particles (potentially inverse grading). Some boulders have bright dots (triangles). (**D**) Close-up of the rough terrain with a brighter part exposed beneath the gravels. Some boulders have bright dots (triangles). (**E**) The boundary area between Muses-C and the rough terrain. Piles of gravel around boulders exist only in the uphill sides of the gravitational slopes (fig. S3). Alignments of boulders (dotted lines) indicate gravel migrations in the direction of the arrow. (**F**) The boundary area close to the Komaba crater showing clear gravel imbrication. (**G**) Frequency distributions of the angles (from horizontal) of the longest axis of gravels in images (B) to (F). Gravels larger than 100 pixels in each image [565, 897, 976, 396, and 426 gravels identified in (B), (C), (D), (E), and (F), respectively] are used to remove the sun-angle bias. Whereas gravel orientations of (C) and (D) are almost random, those of (B), (E), and (F), are clearly organized. The modes of the orientations are plotted as dotted lines. Organization of gravels (or imbrications) is often observed for terrestrial river-bed gravel, where the longest axes are preferentially oriented transverse to the gravel migration (arrows).

We identify three major smooth terrains on Itokawa, the Muses-C, Sagamihara, and Uchinoura regions (Fig. 3D and fig. S1). Although the high-resolution images of smooth terrains (Fig. 3A) were only obtained at one particular portion of the Muses-C region (Fig. 3C), the slight variations in the brightness, surface texture, and color (*6*) of the smooth terrains in distant images indicate that the pebbles observed in Fig. 3A likely cover the rest of the Muses-C region and other smooth terrains uniformly.

The smooth terrains have generally homogeneous and featureless appearances, with a very limited number of craters. The overall slopes of the smooth terrains are typically nonzero but <8°. Detailed observations of the high-resolution images of the Muses-C region provide the following important characteristics: Most of the larger gravels are not buried by pebbles, even at their margins; larger particles, such as cobbles, tend to form clusters (Fig. 3A); and the larger gravels are aligned with directions coincident with the local gravity slope (Fig. 3D). We interpret these as resulting from the substantial vibrations discussed above, because these characteristics are consistent with laboratory experiments in which granular materials show granular convection, typically caused by vertical vibrations (*15*–*17*). Granular convection causes continuous flows of particles sliding down from the top of a convection cell, whose slope angle is within the friction angles of particles (*18*, *19*). Thus, the low slope angles of smooth terrains likely indicate the low friction angles of pebbles, similar to those on Earth (*20*).

Smooth terrains are not randomly distributed on the surface of Itokawa; all of the smooth terrains are in areas of low gravitational plus rotational potential. Moreover, small local lows such as crater floors are commonly filled by smooth materials (Fig. 1, A and D). The locations of both poles match the apexes of domelike shapes in the smooth terrains, which is expected for a slowly rotating body because polar regions will in general be the stable settling point for loose material (*21*). Because the gravitational slopes (Fig. 3D) in the rough terrains are always toward the smooth terrains, the above observations suggest global processes that segregate and migrate the finest gravels to these low points.

Gravel migrations in rough terrains are evidenced by a range of morphological characteristics, as often observed in terrestrial landslide deposits, including imbrications of boulders (Fig. 2, B, E, and F), piles of gravel exclusively on the uphill sides of gravitational slopes (Fig. 2E and fig. S3), larger and often angular boulders with strong alignments (Figs. 2E and 3C), and similarly shaped boulders exhibiting jigsaw-fit textures (Figs. 2E and 3C). The direction of gravel migrations consistently matches with local gravitational slopes (Fig. 3D), supporting the view that migrations are gravity-induced.

Given the dry, vacuum environment on Itokawa, whose escape velocity varies between

10 and 20 cm/s, the migrations discussed above could result from gravel fluidization induced by vibrations (*15*). Vibration can play a major role in the evolution of Itokawa's regolith because Itokawa's small size can keep seismic energy high (Fig. 4A) and because any point on the asteroid is only a short distance from the source of vibration (*22*, *23*). These factors may help keep vibrations active for a relatively long time to support particle fluidization (*22*, *23*). Although the high porosity (~40%) (*24*) and the hypothesized rubble-pile structure (*3*) may substantially attenuate seismic energy, the estimated high restitution value for the Muses-C region (*4*) indicates relatively compacted regolith particles and suggests that seismic attenuation may not be as large. Vibrations might have segregated particles much finer than pebbles into the

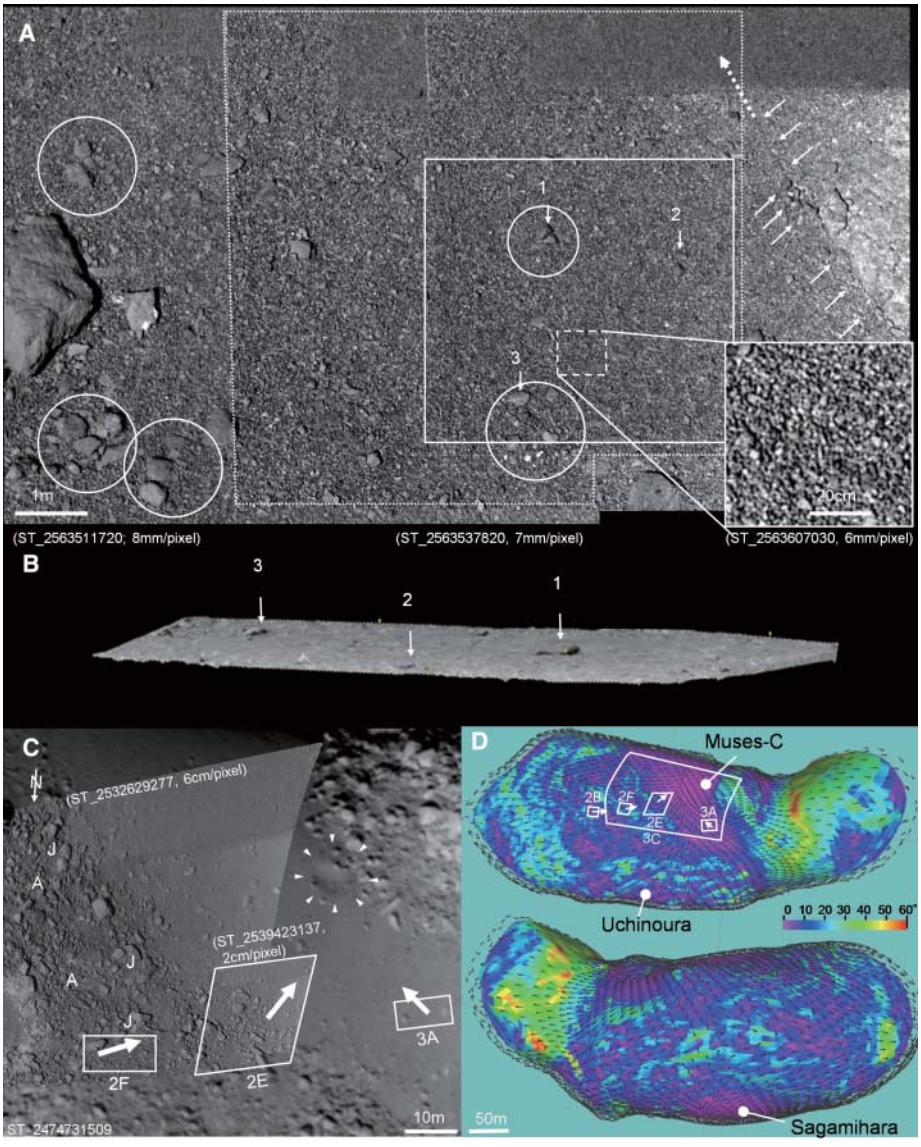

Fig. 3. (**A**) Mosaic of the highest-resolution images in the Muses-C region. The dotted area is overlapped by at least two images, which allows for detailed stereo analyses in (B). Circles indicate clusters of larger gravels. Alignment of cobbles (arrows) indicates the overall gravel migration along the direction of the dotted arrow. The white box shows the area graphically plotted in (B). Boulders with numbers are indicated in (B). (**B**) Three-dimensional model derived from the numerical stereo analyses with more than 11,000 control points. Viewed from the upper right side of (A). Note the flat, featureless surface and the boulders sitting on top of fines in gravitationally stable orientations, which suggests that these boulders are stranded by vibration-induced convections. (**C**) Muses-C and its boundary area. Directions of gravel migrations estimated from morphological characteristics are indicated by arrows. Alignments of boulders A and the jigsaw-fit structures J are identified. A craterlike depression (triangles) is apparently filled by fines. (**D**) The surface slopes (color) and their directions (triangles) computed by combining a polyhedral model of the Itokawa shape and rotation with a constant-density assumption. Note the global trend that the slopes are always toward the smooth terrains. The directions of gravel migrations derived from morphologic characteristics of deposits (arrows) match with those of local slope.

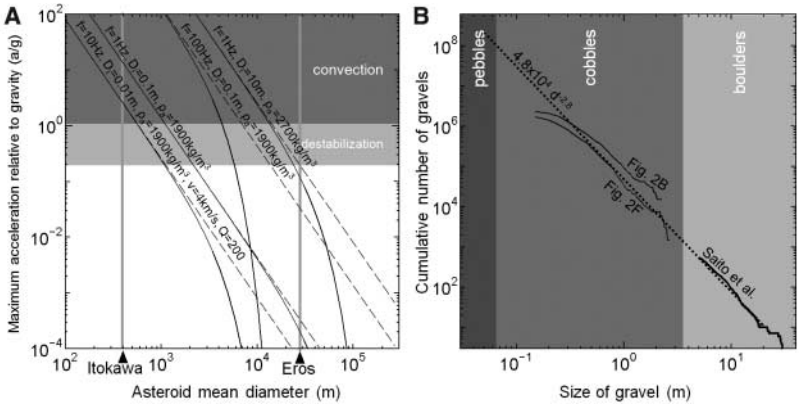

Fig. 4. (**A**) Maximum acceleration of the globally averaged vibration caused by an impact relative to the surface gravity (*a*/*g*) as a function of the size of a stony asteroid. Terrestrial experiments indicate that the gravel destabilization occurred at *a*/*g* ~ 0.2 (*20*) and the granular convection at *a*/*g* slightly larger than unity (*15*). Seismic efficiency, velocity of impact, impactor density, seismic diffusivity, and seismic quality factor are, respectively, 10^{-4}, 5 km^{-1}, 2500 kgm^{-3}, 0.25 km^2s^{-1}, and 2000, except as otherwise noted. These parameter values are given to show the general trend that, for a smaller asteroid, it is easier to achieve a higher *a*/*g* (*27*). (**B**) Preliminary cumulative size distributions (maximum horizontal dimensions) of gravels based on 1150 cobbles in images of Fig. 2, B and F, superimposed on the same plot for 534 boulders in global images (*6*). The distributions generally show a log-log slope of about −2.8 (dotted line), which gives an estimate of the amount of pebbles as 1.9×10^5 m^3 (*27*).

interior, where they can clog the gaps between larger blocks, providing sufficient communication between larger blocks to retain seismic energy while allowing the internal voids to survive.

Particle segregation resulting from migration/vibration is not uncommon in terrestrial laboratory experiments (*17*). Moreover, vibrational size sorting is likely to be more efficient on a smaller body as the threshold velocity for size segregation is theoretically proportional to $\sqrt{g}$ (*25*), where g is the gravity plus rotational acceleration (ranging from 6 to 9 micro-g on Itokawa). Thus, granular convection might not have been limited to the smooth terrains but might have occurred globally. In this case, larger gravels are stranded at the surface to form rough terrains, whereas finer particles migrate beneath and are exposed at potential low areas. Segregation can also be due to other factors. For example, smaller gravels usually have higher mobility because of their lower friction angle (*20*), a smaller mean free path needed for particle migration (*26*), or a smaller amplitude of vibration needed for mobilization, leading to a longer period of migration (*23*). In all cases, variations in particle mobility can explain how gravity-induced global gravel migrations have resulted in the segregation of fines and the formation of smooth terrains, and why boundaries between smooth and rough terrains appear relatively sharp (Fig. 1A).

Our view of Itokawa as a granular mechanical construct is further supported by the total volume of pebbles (2.3×10^5 m^3) (fig. S1) estimated from the total area of smooth terrains (0.075 km^2) (fig. S1). This volume cannot be explained by ejecta from the largest craters on Itokawa but is consistent with those estimated from the cumulative number of boulders (Fig. 4B) (*27*). Thus, pebbles in smooth terrains likely share their origin with boulders in rough terrains. Some cobbles in the close-up images have bright dots on their surfaces (Fig. 2), which are plausibly the remnants of micrometeoroid impact. If so, their number density likely represents the period of time that the cobble is exposed to the space. The number density for a cobble is independent of the roundness or smoothness of the cobble, which varies in each image. This likely indicates that the degradation of cobbles has occurred regardless of their durations of being located at the surface, implying that the cobbles have degraded due not to micrometeoroid impacts but to grindings against other gravels as a result of their collisional histories in orbit or the granular processes discussed above.

References and Notes

1. Regolith is loosely defined as any particulate covering an asteroid. We use the terminology of sedimentary deposits (pebble, cobble, and boulder represent objects whose sizes range from 4 mm to 6.4 cm, 6.4 cm to 2.6 m, and >2.6 m, respectively, with "gravel" including all of them) (*6*).
2. C. R. Chapman, in *Asteroids III*, W. F. Bottke Jr., A. Cellino, P. Paolicchi, R. P. Binzel, Eds. (Univ. Arizona Press, Tucson, 2002) pp. 315–330.
3. A. Fujiwara *et al.*, *Science* **312**, 1330 (2006).
4. H. Yano *et al.*, *Science* **312**, 1350 (2006).
5. T. C. Blair, J. G. McPherson, *J. Sediment. Res.* **69**, 6 (1999).
6. J. Saito *et al.*, *Science* **312**, 1341 (2006).
7. J. E. Richardson, H. J. Melosh, R. Greenberg, *Science* **306**, 1526 (2004).
8. P. C. Thomas, M. S. Robinson, *Nature* **436**, 366 (2005).
9. D. J. Scheeres *et al.*, *Icarus* **8**, 10.1016/j.icarus.2006.12.014 (2007).
10. A. M. Nakamura, A. Fujiwara, T. Kadono, *Planet. Space Sci.* **42**, 1043 (1994).
11. N. Asada, *J. Geophys. Res.* **90**, 2445 (1985).
12. G. J. Flynn, D. D. Durda, *Planet. Space Sci.* **52**, 1129 (2004).
13. P. Lee, *Icarus* **124**, 181 (1996).
14. D. J. Scheeres, *Lunar Planet. Sci. Conf. Abstr.* **XXXVI**, 1919 (2005).
15. H. M. Jaeger, S. R. Nagel, R. P. Behringer, *Rev. Mod. Phys.* **68**, 1259 (1996).
16. A. Rosato, K. J. Strandburg, F. Prinz, R. H. Swendsen, *Phys. Rev. Lett.* **58**, 1038 (1987).
17. J. B. Knight, H. M. Jaeger, S. R. Nagel, *Phys. Rev. Lett.* **70**, 3728 (1993).
18. E. Clement, J. Duran, J. Rajchenbach, *Phys. Rev. Lett.* **69**, 1189 (1992).
19. P. Evesque, J. Rajchenbach, *Phys. Rev. Lett.* **62**, 44 (1989).
20. T. W. Lambe, R. V. Whitman, *Soil Mechanics, SI edition* (Wiley, New York, 1979).
21. V. Guibout, D. J. Scheeres, *Celestial Mech. Dyn. Astron.* **87**, 263 (2003).
22. A. F. Cheng, N. Izenberg, C. R. Chapman, M. T. Zuber, *Meteorit. Planet. Sci.* **37**, 1095 (2002).
23. J. E. Richardson Jr., H. J. Melosh, R. J. Greenberg, D. P. O'Brien, *Icarus* **179**, 325 (2005).
24. S. Abe *et al.*, *Science* **312**, 1344 (2006).
25. E. Asphaug, P. J. King, M. R. Swift, M. R. Merrifield, *32nd Lunar Planet. Sci. Conf. Abstr.*, 1708 (2001).
26. Z. Jiongming, Z. Binglu, W. Bin, *Il Nuovo Cimento* **20**, 1443 (1998).
27. Materials and methods are available as supporting material on *Science* Online.

28. Supported in part by Ministry of Education, Culture, Sports, Science and Technology (MEXT) grant-in-aid 17031005, 2005, and 18740270, 2006 (to H.M.) and in part by Kobe University through the 21st Century Center of Excellence Program: Origin and Evolution of Planetary Systems.

Supporting Online Material

www.sciencemag.org/cgi/content/full/1134390/DC1
Materials and Methods
Figs. S1 to S3
References

28 August 2006; accepted 2 April 2007
Published online 19 April 2007;
10.1126/science.1134390
Include this information when citing this paper.

Molecular Basis of the Shish-Kebab Morphology in Polymer Crystallization

Shuichi Kimata,[1,2] Takashi Sakurai,[1] Yoshinobu Nozue,[1]* Tatsuya Kasahara,[1] Noboru Yamaguchi,[1] Takeshi Karino,[3] Mitsuhiro Shibayama,[3] Julia A. Kornfield[2]*

In the rich and long-standing literature on the flow-induced formation of oriented precursors to polymer crystallization, it is often asserted that the longest, most extended chains are the dominant molecular species in the "shish" of the "shish-kebab" formation. We performed a critical examination of this widely held view, using deuterium labeling to distinguish different chain lengths within an overall distribution. Small-angle neutron-scattering patterns of the differently labeled materials showed that long chains are not overrepresented in the shish relative to their concentration in the material as a whole. We observed that the longest chains play a catalytic role, recruiting other chains adjacent to them into formation of the shish.

With their low cost and wide diversity in polymer chain structures, polyolefins are the most widely used family of synthetic polymers today. As with many polymers, in their solid form they are neither fully crystalline nor amorphous; instead they are considered semicrystalline with a crystal fraction strongly dependent on processing conditions. The morphologies of semicrystalline materials strongly affect their physical properties (*1*), and control of the structural hierarchy from subnanometer- to micrometer-length scales is thus important technologically and fascinating scientifically. The most notable changes in structure and properties are associated with the flow-induced transition from a relatively isotropic, spherulitic morphology to a highly oriented, shish-kebab morphology, which markedly increases stiffness (*2*) and decreases permeability (*1*). This morphological transition is induced by flow and is very sensitive to the molecular attributes of the polymer—particularly those of the longest chains present in the material. Recent advances in catalyst technology afford control of not only the monomer-level structure of the polymer chain (*3*, *4*) but also the topology (*5*) and the nanostructure (*6*) of olefinic polymers. Therefore, there is an increasing impetus to uncover the ways in which these molecular attributes affect flow-induced crystallization.

It is well known that a beautiful superstructure of polymer crystals can be created by crystallization during flow (*7*). This super-

[1]Petrochemicals Research Laboratory, Sumitomo Chemical, 2-1 Kitasode, Sodegaura, Chiba 299-0295, Japan. [2]Division of Chemistry and Chemical Engineering, California Institute of Technology, Pasadena, CA 91125, USA. [3]The Institute for Solid State Physics, The University of Tokyo, Tokai, Naka-gun, Ibaraki 319-1106, Japan.

*To whom correspondence should be addressed. E-mail: nozue@sc.sumitomo-chem.co.jp (Y.N.); jak@caltech.edu (J.A.K.)

Regolith Migration and Sorting on Asteroid Itokawa

Hideaki Miyamoto *et al.*

Science **316**, 1011 (2007);
DOI: 10.1126/science.1134390